Mathematical Optimisation of Magnetic Nanoparticles Diffusion in the Brain White Matter

Tian Yuan[1†*], Yi Yang[2†*], Wenbo Zhan[2*] and Daniele Dini[1*]

[1] *Department of Mechanical Engineering, Imperial College London, SW7 2AZ, UK*
[2] *School of Engineering, King's College, University of Aberdeen, AB24 3UE, UK*
[†] *These authors contributed equally to this work.*
[*] *Correspondence: t.yuan19@imperial.ac.uk (T.Y.), y.yang4.21@abdn.ac.uk(Y.Y.), w.zhan@abdn.ac.uk(W.Z.), d.dini@imperial.ac.uk(D.D.)*

Abstract

Magnetic Nanoparticles (MNPs) is a promising technique to cure brain diseases. On the one hand, by serving as drug carriers, they can bypass the blood-brain barrier and deliver drug molecules to the brain parenchyma; on the other hand, their transport trajectory can be manipulated by applying an external magnetic field. However, due to the complex microstructure of brain tissues, e.g. the anisotropy of white matter (WM), how to achieve desired drug distribution patterns, e.g. uniform distribution, by tuning the drug delivery system is largely unknown. Here, in this study, by adopting a mathematical model capable of capturing the diffusion trajectories of MNPs in the microstructures, we systematically investigated the effects of key parameters in the MNPs delivery system on the equivalent diffusion coefficient of MNPs in the microenvironment of brain WM. The results show that uniform distribution of MNPs in anisotropic tissues can be achieved by adjusting the particle size and magnetic field. We have not only obtained a deeper understanding on how to optimise the MNPs delivery system, it can also be anticipated that an improved mathematical model could even help to achieve complex drug distribution patterns in the complicated brain environment by designing an appropriate combination of the key parameters.
Key words: Brain Diseases; Blood-Brain Barrier; Magnetic Field; Nanoparticle; Drug Delivery

1. Introduction

Degenerative nerve diseases, including Alzheimer's disease and brain cancers, are increasingly threatening human health around the world, particu-

 doi:10.20944/preprints202211.0530.v1

larly for the population over 60 years old [1]. Brain diseases have proven difficult to treat with conventional drug delivery procedures. The disappointing effectiveness is largely due to the limitations of the impermeable nature of the blood-brain barrier (BBB) and the compact microstructure of nerve fibres in the brain white matter (WM) [2]. Encapsulating drugs inside, nanoparticles (NPs) as a vehicle offer great flexibility to optimise size and surface properties that enable drugs to cross the BBB [3, 4]. To date, numerous studies have been conducted to improve the NP fabrication and fine-tune NP properties for enhancing this transvascular transport [5, 6, 7, 8, 9].

However, the latter limitation remains. NP needs to deliver sufficient drugs to the lesion to ensure adequate drug exposure for effective treatment. Its transport in the brain highly depends on the tissue microstructure. The cable-like nerve fibres, as shown in Figure 1, would guide the NPs to undesired directions and locations, resulting in uncontrollable drug distribution and low drug concentration in the target location [10, 11]. This drawback becomes more serious for drug delivery to those lesions embedded in the deep brain tissue.

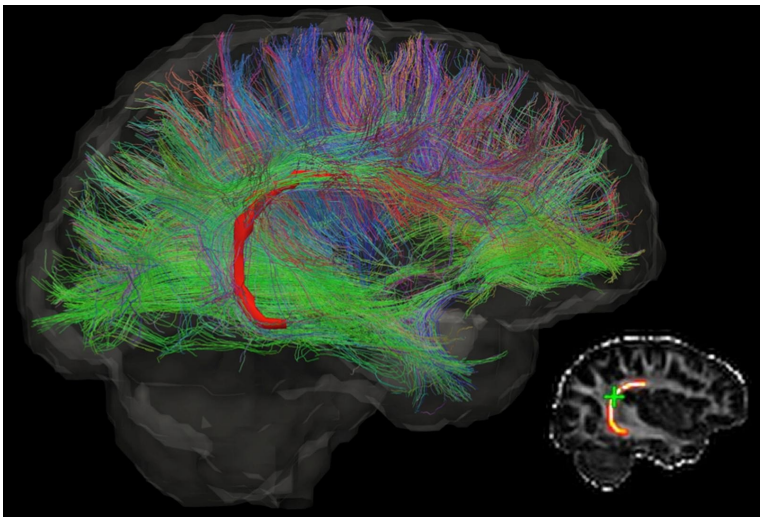

Figure 1: The diffusion tensor image of a brain, which shows the direction of neurons and complexity of the brain microstructure. Different colours indicate different directions. This figure is reprinted from Ref. [12] with open access under the terms of CC BY-NC-ND 4.0 License.

Magnetic nanoparticles (MNPs) that contain a paramagnetic core (e.g. iron oxide) present great potential to overcome the latter limitation, since

 doi:10.20944/preprints202211.0530.v1

their motion can be steered by an externally applied magnetic field [13, 14]. Its feasibility in the treatments of brain circulating system diseases and brain tumours has received some preclinical studies by means of mathematical modelling and experimental observations. For example, Rotariu et al. developed a mathematical model to investigate different techniques to focus small MNPs within the microvasculature of tumours [15]. Sharma et al. mathematically captured the transport behaviours of a cluster of MNPs in a blood vessel to study the application of magnetic drug targeting (MDT) [16]. Kenjeres et al. investigated the concept of the targeted delivery of magnetic pharmaceutical drug aerosols in the human upper and central respiratory system also by mathematical modelling [17]. The fundamental theory of these mathematical models is to calculate the trajectories of MNPs in different environments based on the specific acting forces that determine the NPs' movement, e.g. magnetic force, buoyancy force, and Newton's second law. Regarding experimental studies, except for extensive investigations on coating the Fe_3O_4 NPs by e.g. poly(ethylene glycol) (PEG) and carboxymethyl cellulose (CMC) to increase its capability of BBB penetration, researchers also found that magnetically labelled cancer cells can be killed by magnetic iron-oxide NPs when subjected to oscillating gradients in a strong external magnetic field [18]. More investigations on MNPs' applications are reported in Ref. [19].

All these studies have shown the important role of the magnetic field intensity and topography in manipulating the transport behaviours of MNPs in tissues, blood vessels, and BBB. However, the transport of MNPs in the brain parenchyma is still unclear. The lack of this knowledge would, on the one hand, lead to misjudgement of treatment protocols, on the other hand, limit the development of the MNPs for clinical use, particularly for the treatments against degenerative nerve diseases [20] which mainly occur in nerve fibre-rich WM.

The present study aims to tackle this challenge by investigating the diffusion phenomenon of MNPs in the brain WM. Given mass transport in the brain interstitium is governed by diffusion rather than the bulk movement with the interstitial fluid flow [21], the transport efficiency of the MNPs can be explicitly represented by a diffusion coefficient tensor ($\mathbf{D}$) [22], which can be statistically calculated by monitoring the MNP trajectories [23]. Due to the lack of valid experimental means with ultra-high resolution and a frame rate to directly track the MNPs' movement in deep brain tissue, we adapted a mathematical framework capable of capturing the diffusion pro-

Preprints (www.preprints.org) | NOT PEER-REVIEWED | Posted: 29 November 2022 doi:10.20944/preprints202211.0530.v1

cess of NPs in the brain WM to reproduce the diffusion process of MNPs in an idealised 3D model of brain WM microstructure by further considering the factor of magnetic force. A group of systematic parametric studies were conducted using this model to examine how the key factors of this drug delivery method affect the equivalent diffusion coefficient tensor of MNPs in the brain WM; these include particle size, particle's magnetic property, magnetic field intensity, magnetic field gradient, magnetic field direction, and the tissue microstructure. The results provide feasible strategies to optimise the magnetic NPs-mediated drug delivery to the brain tissues.

2. Materials and Methods

2.1. Mathematical model

Established based on Newton's second law, the mathematical model consists of a set of governing equations for the major forces acting on the NPs, including thermal motion, particle-particle interaction, particle-fluid interaction and particle-axon interaction. Its capability and accuracy of predicting the diffusion coefficient of NPs in the brain WM have been validated and reported in our previous study [24]. In this study, the model was further developed to consider the magnetic force. The mathematical model in this study thus includes the Brownian force (thermal motion, Eq. 1), drag force (resistance due to the fluid viscosity, Eq. 2), and magnetic force (Eq. 3).

$$\mathbf{F}_{\mathrm{B}} = \Phi\sqrt{\frac{12\pi K_{\mathrm{B}}\mu T r_{\mathrm{p}}}{\delta t}} \tag{1}$$

$$\mathbf{F}_{\mathrm{D}} = 6\pi\mu r_{\mathrm{p}}\left(\mathbf{v}_{\mathrm{flow}} - \mathbf{v}_{\mathrm{particle}}\right) \tag{2}$$

$$\mathbf{F}_{\mathrm{M}} = \frac{V\Delta\chi}{\mu_0}(\mathbf{B}\cdot\nabla)\mathbf{B} \tag{3}$$

where $\mathbf{F}_{\mathrm{B}}, \mathbf{F}_{\mathrm{D}}, \mathbf{F}_{\mathrm{M}}$ are the Brownian force, drag force, and magnetic force, respectively. k_{B} is the Boltzmann constant, μ is the dynamic viscosity of the fluid, T is the absolute temperature of the fluid, δt is the time step used to calculate the Brownian force, Φ is a Gaussian random number with zero mean and unit variance to take the randomness of Brownian motion into account, r_{p} is the radius of the particle. $\mathbf{v}_{\mathrm{flow}}$ is the velocity of fluid flow, and $\mathbf{v}_{\mathrm{parlicle}}$ is the velocity of the particle. V is the particle volume, $\Delta\chi$ is the difference in magnetic susceptibilities between the particle and the surrounding medium,

Preprints (www.preprints.org) | NOT PEER-REVIEWED | Posted: 29 November 2022 doi:10.20944/preprints202211.0530.v1

$\mu_0 = 4\pi \times 10^{-7} H/m$ is the permeability of vacuum, and $\mathbf{B}$ is the applied magnetic field.

Since this study is focused on the diffusion phenomenon only, the fluid was assumed to be static, i.e., $\mathbf{v}_{\text{flow}} = 0$. Obeying Newton's second law, the displacement of a particle i is:

$$d\mathbf{r_i} = \left[\sum_{i=1}^{N} (\mathbf{F}_{\text{B}i} + \mathbf{F}_{\text{D}i} + \mathbf{F}_{\text{M}i})\right] (\Delta t)^2 \tag{4}$$

where $d\mathbf{r_i} = (dx_i, dy_i, dz_i)^T$ is the displacement vector of the i th particle, Δt is the time step. The equivalent diffusion coefficient in x direction can be then obtained by:

$$D_{xx} = \left\langle R_{xx}^2 \right\rangle / 2t \tag{5}$$

$$\left\langle R_{xx}^2 \right\rangle = \sum_{i=1}^{n} (dxx_i)^2 \tag{6}$$

where $\langle R_{xx}^2 \rangle$ is the average of mean square displacement (MSD) of all the particles in X direction . dxx is the displacement of a NP in x direction. n is the number of NPs in the system. t is the diffusion time.

The equivalent diffusion coefficients in the Y and Z directions have the same definition in Eq. 5 and Eq. 6 using the parameters for the Y and Z directions, respectively. Please note that the main axis of the coordinate system is placed parallel to the axon tracts in the computation domain. This enables using the diffusion ellipsoid in which only the three diagonal elements of D_{xx}, D_{yy} and D_{zz}, are needed.

2.2. Geometric model

The 3D geometry of the brain WM microstructure was reconstructed by sweeping a representative cross-sectional geometry of brain WM [24] along the axon tracts. Fig. 1 of Ref. [25] shows that axons appear "wavy" or undulated under in situ length conditions when visualised using neurofilament immunohistochemistry. We, therefore, reconstructed the 3D microstructure as shown in Figure 2A (model dimension: 20 μm $\times$ 20 μm $\times$ 20 μm). Tortuosity (τ) is an important geometric parameter that describes the longitudinal shape of axons. It is defined as the ratio of axon length to the distance between the axon's two endpoints. The statistical data of axon tortuosity obtained in Ref. [26] demonstrates that most axons have tortuosity ranging

Preprints (www.preprints.org) | NOT PEER-REVIEWED | Posted: 29 November 2022 doi:10.20944/preprints202211.0530.v1

from 1.0 (i.e. straight) to 1.3. The average distance between axons is 100 nm and the tissue porosity is about 0.3, both of which are located in the experimental range [27, 28]. Based on this information, we reconstructed the 3D geometry. Details on generating a representative cross-sectional MW geometry are reported in Ref. [24].

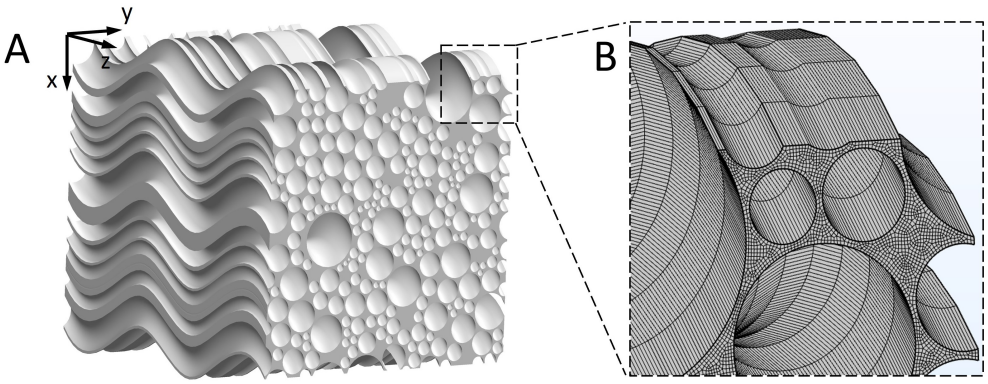

Figure 2: 3D reconstruction of the WM microstructure. A. Reconstructed microstructure of the brain WM. B. Finite element mesh of the microstructure.

2.3. Material properties

Although we did not consider the fluid flow, the fluid's viscosity is important to the particle diffusion behaviours. We thus adopted the viscosity of measured interstitial fluid $3.5 \times 10^{-3} Pa \cdot s$ [29]. Based on the practical applications of NPs used to treat brain diseases [30, 2], the NPs' size normally does not exceed 100 nm, because measurements show that the distance between neurons is within 38-64 nm [27]. Therefore, in this study, NPs with the diameters of 10 nm, 30 nm, 50 nm, 70 nm, and 90 nm, were investigated. It is worth noting that the magnetic susceptibility of MNPs is not constant and highly dependent on the particle size, e.g. MNP smaller than 50 nm can be super-paramagnetic ($\chi \gg 1$) [31]. In order to capture the complex effect of the numerous parameters (magnetic field intensity (B), the gradient of magnetic field intensity ∇B, particle size (d), and magnetic susceptibility (χ)), while themselves are mutually coupled, here we introduce a new parameter: magnetic force density ($f = \chi B \nabla B / \mu_0$ $[N/m^3]$). The advantage is that the parametric study can be significantly simplified by reducing the number of parameters needed to capture the physical system. Furthermore, from the aspect of clinical applications, the values of $\chi, B,$ and ∇B can be freely

 doi:10.20944/preprints202211.0530.v1

chosen only if they satisfy the value of $\mu_0 f$ (note that μ_0 is the permeability of vacuum, a constant value), which also significantly simplifies the clinical protocols. The rest of the parameters include temperature (310 K - normal body temperature) and Boltzmann's constant ($k_B = 1.38 \times 10^{-23} J/K$ [32]).

2.4. Boundary conditions

The particles were assumed to undergo diffuse scattering when they hit the axons and would move out of the computational domain when they reach the boundaries [24]. The biochemical interactions between the axons and MNPs, e.g., endocytosis were not considered as this study focus on the measurement of diffusion coefficient.

2.5. Simulation setup

The hex element was adopted to mesh the microstructural geometry, as shown in Figure 2D. According to the mesh sensitivity test, the gaps between axons should contain at least two meshes, which was the criteria for choosing element size in this study. About 1,240,000 elements were created in the geometric models. At $t = 0s$, 125,000 MNPs were released from a cubic domain at the centre of the model to mimic the transportation process of drug molecules from the injection site. This number of NPs is selected after a sensitivity study, which is adequate to obtain statistically stable results for calculating the MSD as defined in Eq. 6. Note that capturing the Brownian motion needs a fine time step, which also depends on the size of particles, so time-step tests are essential in different occasions before choosing the value of the time step. We also conducted time-step independence tests for each model. COMSOL Multiphysics 6.0 software was used to solve the mathematical model and calculate the trajectories of the MNPs. The linear solver is set as Multifrontal Massively Parallel Sparse direct solver (MUMPS) and the Automatic Newton method is chosen as the nonlinear solver [33].

3. Results

We first present MNPs' diffusion behaviours under the baseline delivery conditions to show how the external magnetic field controls the MNP trajectory. This is followed by the analyses of the individual effect of particle size, magnetic force density, axon shape (tortuosity) and magnetic field direction on the diffusion coefficient tensor.

Preprints (www.preprints.org) | NOT PEER-REVIEWED | Posted: 29 November 2022 doi:10.20944/preprints202211.0530.v1

3.1. Diffusion behaviours of MNPs in the brain WM

We monitored diffusion behaviours of 50 nm MNPs under three conditions, namely $f = 0$ (no external magnetic field), $f = 2000/\mu_0$, and $f = 4000/\mu_0$, respectively, which are located in the practical ranges, since the maximum values of practically applied B, ∇B, and χ could reach 10 T, 100 T/m, and 200,000, respectively [34, 35, 36], the values of 2000 and 4000 are within the application range. To focus on the impact of the external magnetic field, the geometry with $\tau = 1$ was adopted. Figures 3A1 $\sim$ 3C1 show the MSD of the MNPs under these three conditions as a function of time, respectively. To more clearly interpret the mechanism behind the curves, figures 3A2$\sim$3C2 and 3A3$\sim$3C3 present the final distributions of the MNPs (t=0.08 s) from the top view and side view of the computational domain.

A rapid increase of MSD can be found in all directions at the beginning of diffusion owing to the dense MNPs and violent collisions between the MNPs. With the MNPs dispersing into the domain, interactions determining the particle motion would gradually reach dynamic equilibrium. This leads to a stable diffusion phase which is reflected as a linear increase in MSD with time, as shown in Figures 3A1 $\sim$ 3C1, where the slop can be used to calculate the equivalent diffusion coefficient (Eq. 5). Comparisons between the time courses of MSD demonstrate the significant impacts of external magnetic field on the $\mathbf{D}$ of MNPs. D_{zz} is much greater than D_{xx} and D_{yy} when no external magnetic field is applied. This is because MNPs in the Z direction would experience less resistance that is induced by the presence of axons, as shown in Figure 3A3. D_{xx} and D_{yy} are almost equal, since the microstructure of the brain WM is nearly isotropic in the transverse plane, as shown in Figure 3A2. Moreover, the external magnetic field in the XY direction can greatly increase D_{xx} and D_{yy}. Figures 3B1 and 3C1 show that $D_{xx} = D_{yy} \approx D_{zz}$ when $f = 2000/\mu_0$ and $D_{xx} = D_{yy} > D_{zz}$ when $f = 4000/\mu_0$. Therefore, the MNPs' displacement in the XY direction increases with f (Figure 3A2 $\sim$ 3C2), resulting in the MNPs distribution becoming more spherical, as shown in Figures 3A3 $\sim$ 3C3).

Preprints (www.preprints.org) | NOT PEER-REVIEWED | Posted: 29 November 2022 doi:10.20944/preprints202211.0530.v1

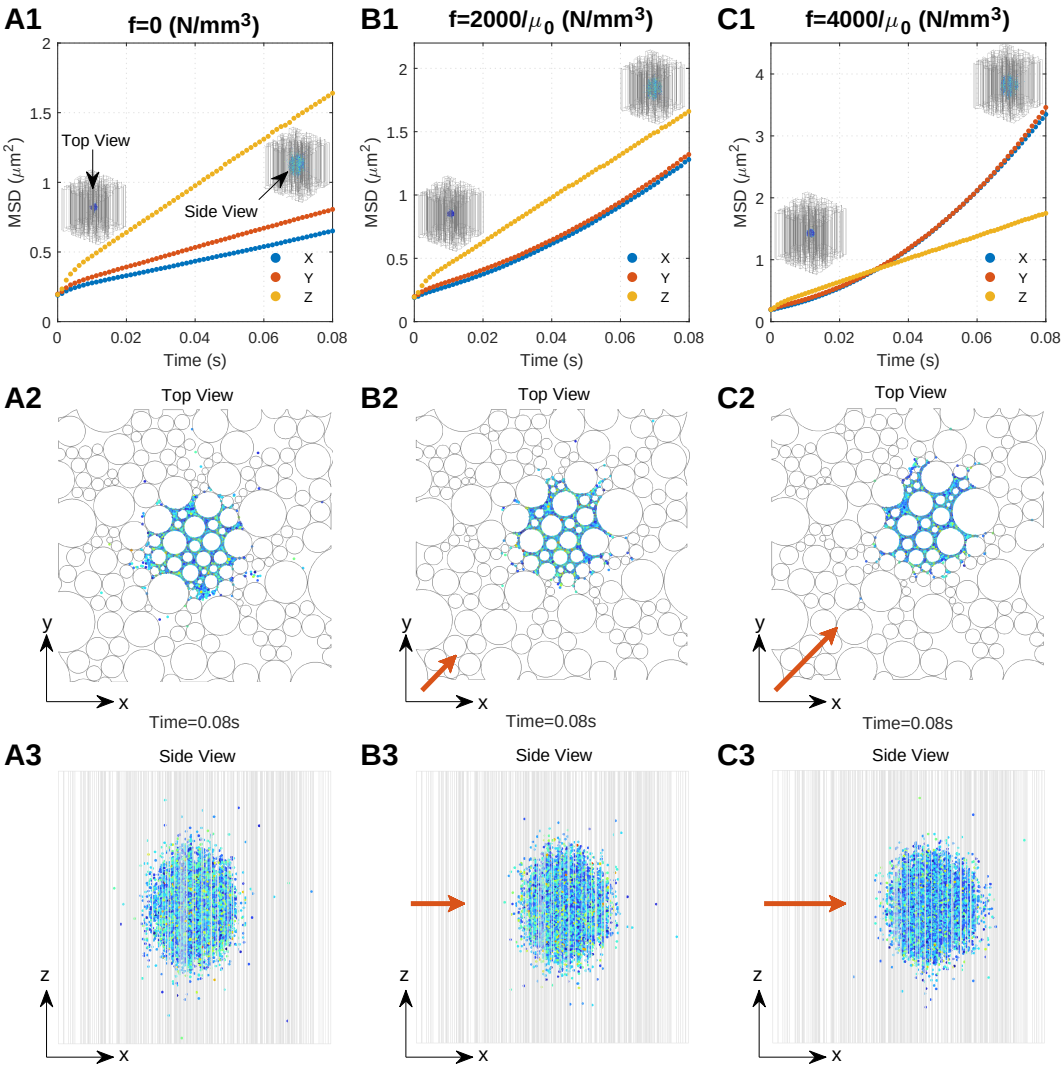

Figure 3: Typical diffusion behaviours of the MNPs in the brain WM under different conditions. Series A. Results when there is no external magnetic field. A1. Relationship between MSD and time. A2. Top view of MNPs distribution. A3. Side view of the MNPs distribution. Series B. Results when the magnetic force density is $2000/\mu_0$. B1. Relationship between MSD and time. B2. Top view of MNPs distribution. B3. Side view of the MNPs distribution. Series C. Results when the magnetic force density is $4000/\mu_0$. C1. Relationship between MSD and time. C2. Top view of MNPs distribution. C3. Side view of the MNPs distribution. The directions of the top view and side view are shown in Figure A1 and the direction of the applied magnetic field is shown by the orange arrows with their lengths proportional to the magnetic field intensity.

Preprints (www.preprints.org) | NOT PEER-REVIEWED | Posted: 29 November 2022 doi:10.20944/preprints202211.0530.v1

3.2. Effect of particle size and magnetic force density

Figure 4A $\sim$ 4E show the effect of magnetic force density on the **D** of MNPs with different sizes. For convenience, we set the horizontal axis as $\mu_0 f$ as it equals $\chi B \nabla B$ and thus can directly determine the magnetic field and susceptibility of MNPs. We could obtain the following results by comparing results in these figures:

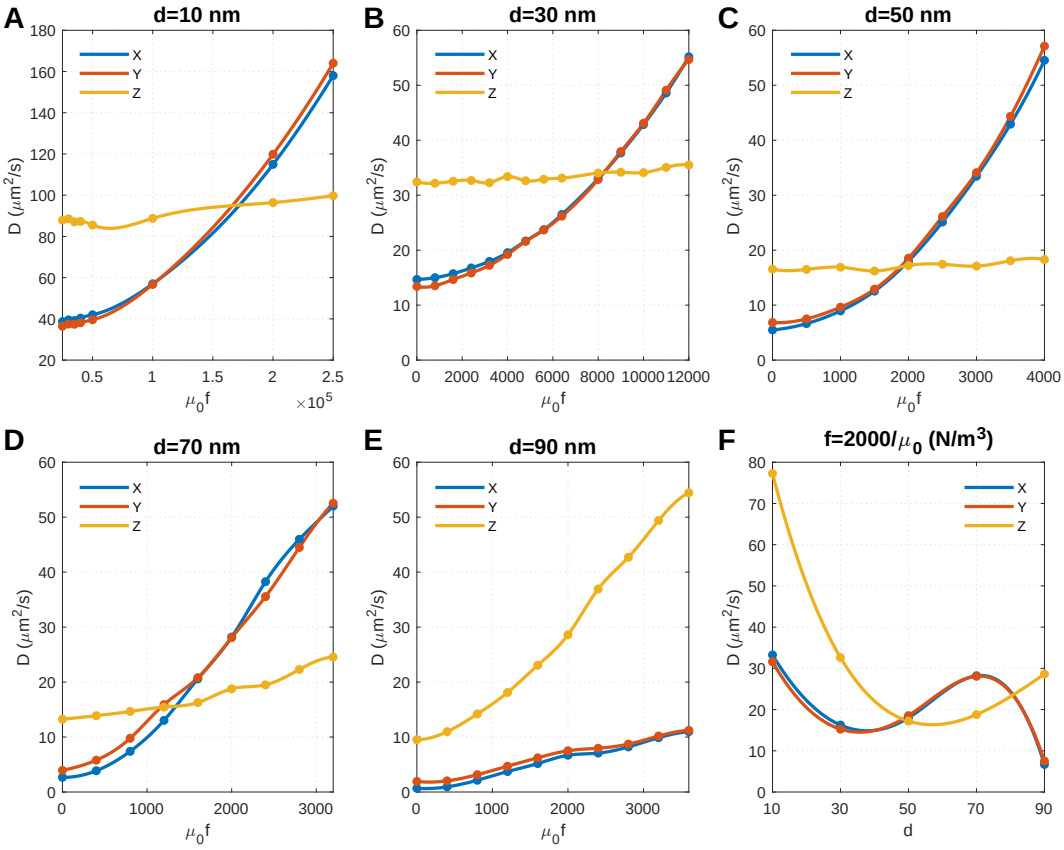

Figure 4: Effect of particle size and magnetic force density on the diffusion coefficients of MNPs. A-E show the results of MNPs with diameters of 10 nm, 30 nm, 50 nm, 70 nm, 90 nm, respectively. Note that MNPs with different particle sizes have different kinetic energies under the same magnetic force density, so different magnetic force densities were applied to MNPs with different particle sizes in order to capture the points where diffusion coefficients in X and Y directions are equal to that in Z direction. F. Relationship between diffusion coefficients and particle size when the magnetic force density is $2000/\mu_0$.

1. When $f = 0$ (i.e., without external magnetic field), **D** decreases with

 doi:10.20944/preprints202211.0530.v1

the particle size due to the decreased ratio of Brownian force (Eq. 1) to drag force (Eq. 2).

2. The size of MNPs plays a key role. For the MNPs with a size ranging from 10 nm to 70 nm, the external magnetic field can override the impact of axons and result in an isotropic $\mathbf{D}$ (i.e., $D_{xx} = D_{yy} = D_{zz}$). Comparisons further show a lower magnetic force density is required for larger MNPs to achieve an isotropic $\mathbf{D}$. The magnitude of isotropic diffusivity is also found to be reversely correlated to particle size.
3. The diffusion anisotropy of 90 nm MNPs increases with the magnetic force density, indicating an isotropic $\mathbf{D}$ does not exist. This is because the MNPs with a comparable dimension as the average distance between axons (100nm in this geometry model) are difficult to transversely diffuse in the space between axons (see the initial points in Figure 4E which shows low D_{xx} and D_{yy}). Increasing the magnetic force density would accelerate the MNPs and lead to more violent collisions between the MNPs and the axons. Although this increases the velocity of MNPs that successfully pass through the gaps between axons and lead to increased D_{xx} and D_{yy}, more MNPs would be blocked due to their higher velocity and more violent collisions with the axons; these parts of accelerated MNPs would then turn to Z direction, thus dramatically increasing D_{zz} and the diffusion anisotropy.
4. The impact of collisions with axons can also be found for 70 nm MNPs, as the component of diffusion coefficient in the Z direction (D_{zz}) significantly increases with the magnetic force density. Because the MNPs are still smaller than the average distance between axons, the rebound particles can transport in all three directions of X, Y and Z. Since it is a random event whether the x-component overpowers the y-component, D_{xx} and D_{yy} alternately outpace each other, as shown in Figure 4D.

Figure 4C shows that increasing magnetic force density has a significantly limited effect on 50 nm MNPs, and the isotropic $\mathbf{D}$ could be achieved when $\chi B \nabla B = 2000$. We chose $f = 2000/\mu_0$ to draw the relationship between particle size and $\mathbf{D}$ and found that the isotropic $\mathbf{D}$ could also be achieved when $d \approx 80nm$ under the same magnetic force density, which provides more flexibility to clinical applications.

3.3. Effect of axon shape (tortuosity) and magnetic force density

As shown in Figure 1B, the majority of axons have their tortuosities ranging from 1 to 1.3. Therefore, in this study, we conducted studies in

Preprints (www.preprints.org) | NOT PEER-REVIEWED | Posted: 29 November 2022 doi:10.20944/preprints202211.0530.v1

microstructures with 4 different tortuosities, namely $\tau = 1.0, 1.1, 1.2, 1.3$, respectively. Figure 5 shows the effect of magnetic force density on the **D** in different microstructures. To focus on the effect of axon shape, the MNP size was fixed at 50 nm. The direction of the magnetic field was perpendicular to the Z direction.

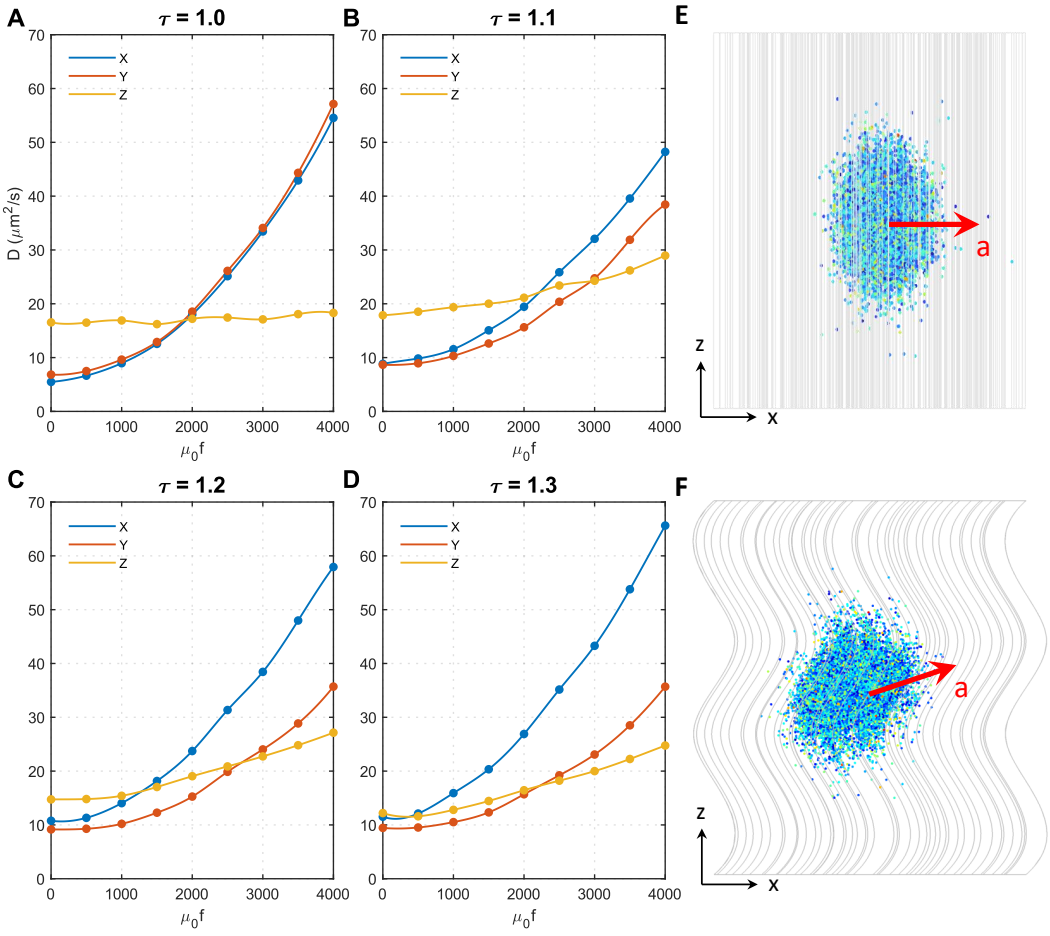

Figure 5: Effect of axon shape (tortuosity) and magnetic force density on the diffusion coefficients of MNPs. A-D show the results of axon shape with the tortuosity of 1.0, 1.1, 1.2, 1.3, respectively E. The acceleration direction of 50 nm MNPs in microstructure with $\tau = 1.0$. F. The acceleration direction of 50 nm MNPs in microstructures with $\tau > 1.0$.

Initially, when $f = 0$, $D_{xx} \approx D_{yy} < D_{zz}$ in all microstructures, but the difference significantly decreases with the tortuosity; when $\tau = 1.3$, D_{xx} and D_{yy} are even comparable to D_{zz}, which means the approximately isotropic diffu-

Preprints (www.preprints.org) | NOT PEER-REVIEWED | Posted: 29 November 2022 doi:10.20944/preprints202211.0530.v1

sion can be automatically achieved. The effect of τ becomes more complex after applying the external magnetic field. $D_{xx} \approx D_{yy}$ always holds for $\tau = 1.0$ regardless of the magnetic force density. In contrast, D_{xx} increases faster with the magnetic force density compared to D_{yy} when $\tau > 1.0$. This is because only the MNP movement in the XY direction was accelerated when $\tau = 1.0$, as shown in Figure 5E, whereas the diffusion in the Z direction was less affected (see Figure 5A). However, when $\tau > 1.0$, as axons bend towards the X direction in the present microstructures reconstructed based on Fig. 1 of Ref. [25], the MNPs can more easily turn direction and move along the axon tracts when encountering resistance in XY direction. Under this condition, the acceleration direction is in XY direction but slightly to the Z direction, as shown in Figure 5F. This trend can be enhanced by either increasing resistance in XY direction (i.e., acceleration introduced by higher f) or making the axons closer to x direction (i.e., increasing tau). These explain why D_{zz} in Figures 5B $\sim$ 5D increases with f and increases more sharply with τ. Furthermore, as axons bend to X direction in the reconstructed microstructures, the derivative Z acceleration has x component, thus making $D_{xx} > D_{yy}$. This effect is enhanced with tortuosity, so the difference between D_{xx} and D_{yy} also increases with tortuosity.

3.4. Effect of magnetic field direction and magnetic force density

As analysed above, the unexpected anisotropy in X and Y directions is due to the change of acceleration direction, which is caused by axon bending (see Figure 5F). In the following studies, we tried to change the direction of the magnetic field to minimise this effect. Shown in Figure 6 are the effects of magnetic field direction on **D**s of 50 nm MNPs in the microstructures with different tortuosity. The direction of the magnetic field is perpendicular to the Z direction in the top panels and perpendicular to the local axon tracts in the bottom panels.

Preprints (www.preprints.org) | NOT PEER-REVIEWED | Posted: 29 November 2022 doi:10.20944/preprints202211.0530.v1

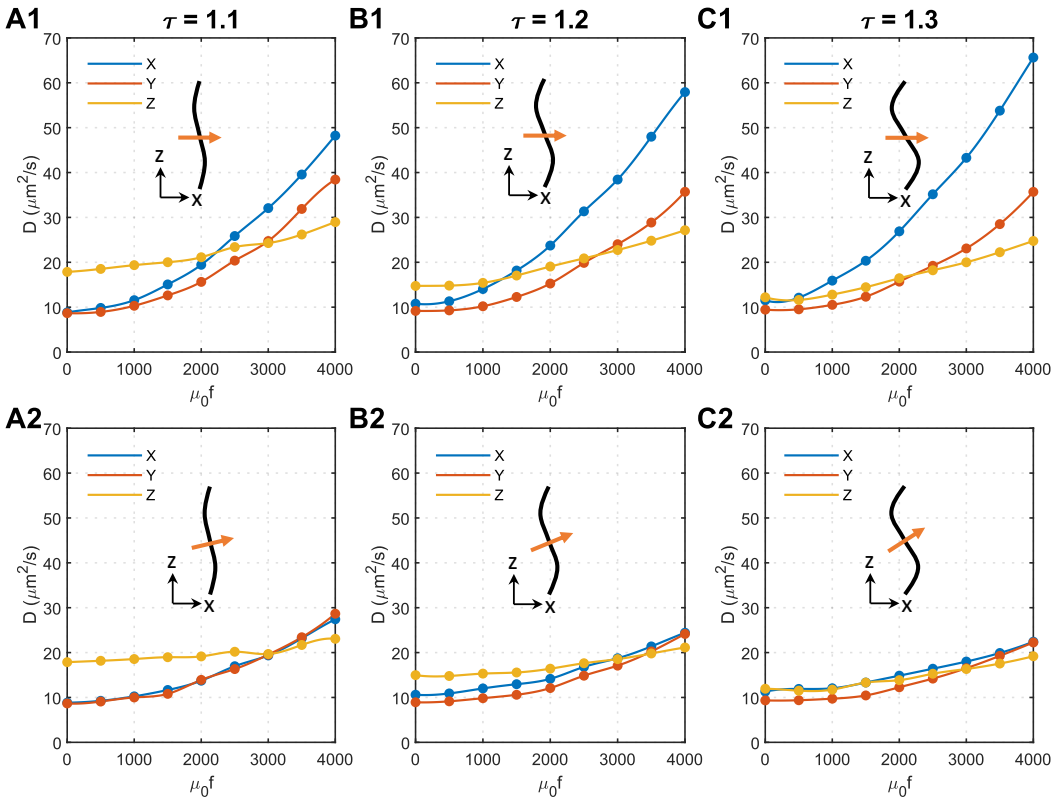

Figure 6: Effect of magnetic field direction on the anisotropy of MNPs diffusion coefficients in the brain WM. A1. Tortuosity=1.1, the magnetic field is perpendicular to Z direction. A2. Tortuosity=1.1, the magnetic field is perpendicular to the axons. B1. Tortuosity=1.2, magnetic field is perpendicular to Z direction. B2. Tortuosity=1.2, the magnetic field is perpendicular to the axons. C1. Tortuosity=1.3, the magnetic field is perpendicular to Z direction. C2. Tortuosity=1.3, magnetic field is perpendicular to the axons. In each figure, the black curve represents the axon shape while the orange arrow shows the direction of the applied magnetic field.

As shown in Figures 6A2 $\sim$ 6C2, applying the magnetic field perpendicular to the local axons can effectively eliminate the anisotropy of the diffusion coefficient in the X and Y directions. Regardless of the axon shape, the isotropic $D \approx 20\ \mu m^2/s$ can be achieved in all the tested microstructures using similar magnetic force densities of approximately $3000/\mu_0$. The comparison with Figures 6A1 $\sim$ 6C1 denotes that tortuosity has a limited impact on how the external magnetic field manipulates the MNPs in the brain WM when the magnetic field is perpendicular to the local axons.

Preprints (www.preprints.org) | NOT PEER-REVIEWED | Posted: 29 November 2022 doi:10.20944/preprints202211.0530.v1

4. Discussion

In the absence of advanced imaging techniques to precisely capture the diffusion behaviours of MNPs manipulated by an external magnetic field *in vivo*, we adapted a mathematical model to capture the controlled diffusion behaviours of MNPs in 3D microstructures under the external magnetic field. The parametric studies conducted in this study based on the mathematical model provide important qualitative insights into how the major parameters in the delivery system affect the diffusion behaviours of the MNPs in brain WM, which possesses great clinical importance [37, 38]. So far, we have shown that the diffusion coefficient of NPs in the brain WM can be significantly increased by surface charge [24] and their diffusion direction can be controlled by applying MNPs together with the external magnetic field.

While greater attention has been paid to improving the chemical and biological performances of NPs, e.g. reducing drug elimination rate [39] and increasing cytotoxic effects [40], to enhance the effectiveness of NPs, we found that the MNP size and external magnetic field are of vital importance to achieve desired spatial distribution of MNPs in the brain microstructure. Instead of identifying the individual impact of each factor, we found that the particle magnetic susceptibility (χ), magnetic field intensity (B) and its gradient (∇B) would work as a group with the factor of particle size (d) to influence the MNPs diffusion. Results from this study provide flexibility to achieve the desired diffusion phenomenon by optimising the combination of the abovementioned factors which can suit the clinical practice best. For instance, although a much higher magnetic force density is required to drive smaller MNPs to reach uniform distribution (see Figure 4), the magnetic field intensity and its gradient may not necessarily need to increase because smaller MNPs could have a much higher magnetic susceptibility [41] (see Eq. 3). Moreover, the modelling results also demonstrated that if the particle size is much smaller than the gaps between axons, applying an external magnetic field perpendicular to the local axons enables isotropic diffusion. However, an isotropic $\mathbf{D}$ may not exist if the particle size is comparable to the gaps between axons, since the applied external magnetic field would drastically increase D_{zz} over D_{xx} and D_{yy}. Although magnetic tools may not be able to help large MNPs achieve uniform distribution in WM, it is still feasible to increase their transverse penetration as D_{xx} and D_{yy} are increasing with the magnetic force density. One needs to note that the tissue microstructure can vary considerably between individuals, depending on the location of the

 doi:10.20944/preprints202211.0530.v1

lesion in the brain, the patient's age, gender and disease stage, etc. Such complexity would require a personalized treatment plan to maximize the delivery outcomes.

Figures 5 and 6 show that although axons' tortuosity together with the magnetic force density enhances the transverse diffusion anisotropy of MNPs in WM, placing the magnetic field perpendicular to the local axons can make the diffusion coefficient isotropic. For the situation as shown in Fig. 1 of Ref. [25], more attention should be paid to adjusting the direction of the applied magnetic field. However, in some other regions, where axon bending direction is more random, transverse anisotropy introduced by axons' tortuosity may not be as significant as it appears in this study. With the aid of the Diffusion Tensor Imaging (DTI) technique [42], the principal direction of axon tracts can be obtained. This can be used as a key reference to determine the direction when applying an external magnetic field.

Finally, some assumptions in the present study deserve further discussion. Regarding the mathematical and geometrical models, several factors that can also affect the transport of MNPs in the brain WM are not taken into account; these include the water transport across the cell membrane, hydrophobic nature of large biomolecules, the variation of local fluid viscosity due to the components in the extracellular matrix, and MNP-cell adhesion. This is mainly because there is a lack of mathematical models that can accurately describe and reconcile these complex processes. Further support from experiments is also needed to establish appropriate models for these processes in future. The WM cross-sectional is swept along the axon tract to generate the 3D microstructure, as shown in Figure 2. The realistic 3D structure could be more complex and the directions of the axons may not be so uniform, depending on the location in the brain. However, as the aim of this study is to qualitatively understand the effects of parameters of the magnetic system on the diffusion tensor of MNPs, the representative microstructure is enough to provide key findings. 3D realistic microstructures rebuilt from the microscopic images can be used in future studies on specific degenerative nerve diseases. By continuously improving this mathematical framework, we anticipate that we will be able to precisely tune the diffusion coefficient and diffusion direction of NPs, which would remarkably increase the efficiency of delivering nano-drugs into the deep brain tissues.

 doi:10.20944/preprints202211.0530.v1

5. Conclusions

In summary, this modelling framework enables us to gain a deeper understanding on (i) 3D diffusion behaviours of MNPs in brain WM and the corresponding diffusion coefficient tensors, (ii) how MNPs diffusion behaviours in the anisotropic tissue can be manipulated by the externally applied magnetic field, and (iii) how particle size, particle susceptibility, magnitude and direction of the externally applied magnetic field, and axons shape affect the MNPs' equivalent diffusion coefficient tensors. The following key findings were obtained from the results of the present study:

1. Applying an external magnetic field could achieve uniform distribution (isotropic **D**) of MNPs in anisotropic tissues when the particle size is much smaller than the gaps between cells. We thus anticipate that applying a complex magnetic field may potentially be able to design the spatial distribution pattern.
2. When the particle size is comparable to the gaps between cells, isotropic **D** of MNPs cannot be achieved. The anisotropy even increases with the external magnetic field.
3. Special attention is suggested to be paid to the particle size, as the seletion of particle size would affect the settings of nearly all the other key parameters in the whole system.
4. The magnetic field is suggested to be perpendicular to the local axon tracts to eliminate the transverse anisotropy of **D** induced by the axons' tortuosity.
5. The parameter $\chi B \nabla B$ (equal to f/μ_o) could work as a derived parameter to influence the MNPs' equivalent diffusion coefficient tensor. Adopting this derived parameter would provide more flexibility to the practical applications.

Acknowledgements

This project has received funding from the European Unions Horizon 2020 research and innovation programme under Grant Agreement No. 688279. Daniele Dini would like to acknowledge the support received from the EPSRC under the Established Career Fellowship Grant No. EP/N025954/1. Wenbo Zhan would like to acknowledge the support received from the Children with Cancer UK under the project Children's Brain Tumour Drug Delivery Consortium Grant No. 16-224.

References

[1] D. V. Telegina, O. S. Kozhevnikova, N. G. Kolosova, Changes in Retinal Glial Cells with Age and during Development of Age-Related Macular Degeneration, Biochemistry (Mosc.) 83 (9) (2018) 1009–1017. doi:10.1134/S000629791809002X.

[2] W. Li, J. Qiu, X.-L. Li, S. Aday, J. Zhang, G. Conley, J. Xu, J. Joseph, H. Lan, R. Langer, R. Mannix, J. M. Karp, N. Joshi, BBB pathophysiology–independent delivery of siRNA in traumatic brain injury, Sci. Adv. 7 (1) (2021) eabd6889. doi:10.1126/sciadv.abd6889.

[3] G. Leyva-Gómez, H. Cortés, J. J. Magaña, N. Leyva-García, D. Quintanar-Guerrero, B. Florán, Nanoparticle technology for treatment of Parkinson's disease: the role of surface phenomena in reaching the brain, Drug Discovery Today 20 (7) (2015) 824–837. doi:10.1016/j.drudis.2015.02.009.

[4] C. Saraiva, C. Praça, R. Ferreira, T. Santos, L. Ferreira, L. Bernardino, Nanoparticle-mediated brain drug delivery: Overcoming blood–brain barrier to treat neurodegenerative diseases, J. Controlled Release 235 (2016) 34–47. doi:10.1016/j.jconrel.2016.05.044.

[5] S. Honary, F. Zahir, Effect of Zeta Potential on the Properties of Nano-Drug Delivery Systems - A Review (Part 1), Trop. J. Pharm. Res. 12 (2) (2013) 255–264. doi:10.4314/tjpr.v12i2.19.

[6] G. C. Terstappen, A. H. Meyer, R. D. Bell, W. Zhang, Strategies for delivering therapeutics across the blood–brain barrier, Nat. Rev. Drug Discovery 20 (2021) 362–383. doi:10.1038/s41573-021-00139-y.

[7] D. Lundy, K.-J. Lee, I.-C. Peng, C.-H. Hsu, J.-H. Lin, K.-H. Chen, Y.-W. Tien, P. C. H. Hsieh, Inducing a Transient Increase in Blood–Brain Barrier Permeability for Improved Liposomal Drug Therapy of Glioblastoma Multiforme, ACS Nano 13 (1) (2019) 97–113. doi:10.1021/acsnano.8b03785.

[8] J. Xie, Z. Shen, Y. Anraku, K. Kataoka, X. Chen, Nanomaterial-based blood-brain-barrier (BBB) crossing strategies, Biomaterials 224 (2019) 119491. doi:10.1016/j.biomaterials.2019.119491.

[9] Y. Yang, W. Zhan, Role of Tissue Hydraulic Permeability in Convection-Enhanced Delivery of Nanoparticle-Encapsulated Chemotherapy Drugs to Brain Tumour, Pharm. Res. 39 (5) (2022) 877–892. arXiv:35474156, doi:10.1007/s11095-022-03261-7.

[10] T. Yuan, W. Zhan, A. Jamal, D. Dini, On the microstructurally driven heterogeneous response of brain white matter to drug infusion pressure, Biomech. Model. Mechanobiol. 21 (4) (2022) 1299–1316. doi:10.1007/s10237-022-01592-3.

[11] A. Jamal, T. Yuan, S. Galvan, A. Castellano, M. Riva, R. Secoli, A. Falini, L. Bello, F. Rodriguez y. Baena, D. Dini, Insights into Infusion-Based Targeted Drug Delivery in the Brain: Perspectives, Challenges and Opportunities, Int. J. Mol. Sci. 23 (6) (2022) 3139. doi:10.3390/ijms23063139.

[12] E. Moore, R. S. Schaefer, M. E. Bastin, N. Roberts, K. Overy, Diffusion tensor MRI tractography reveals increased fractional anisotropy (FA) in arcuate fasciculus following music-cued motor training, Brain Cogn. 116 (2017) 40–46. doi:10.1016/j.bandc.2017.05.001.

[13] L. Zwi-Dantsis, B. Wang, C. Marijon, S. Zonetti, A. Ferrini, L. Massi, D. J. Stuckey, C. M. Terracciano, M. M. Stevens, Remote Magnetic Nanoparticle Manipulation Enables the Dynamic Patterning of Cardiac Tissues, Adv. Mater. 32 (6) (2020) 1904598. doi:10.1002/adma.201904598.

[14] S. Luo, C. Ma, M.-Q. Zhu, W.-N. Ju, Y. Yang, X. Wang, Application of Iron Oxide Nanoparticles in the Diagnosis and Treatment of Neurodegenerative Diseases With Emphasis on Alzheimer's Disease, Front. Cell. Neurosci. 14 (2020). doi:10.3389/fncel.2020.00021.

[15] O. Rotariu, N. J. C. Strachan, Modelling magnetic carrier particle targeting in the tumor microvasculature for cancer treatment, J. Magn. Magn. Mater. 293 (1) (2005) 639–646. doi:10.1016/j.jmmm.2005.01.081.

[16] S. Sharma, V. K. Katiyar, U. Singh, Mathematical modelling for trajectories of magnetic nanoparticles in a blood vessel under magnetic field, J.

Magn. Magn. Mater. 379 (2015) 102–107. doi:10.1016/j.jmmm.2014.12.012.

[17] S. Kenjereš, J. L. Tjin, Numerical simulations of targeted delivery of magnetic drug aerosols in the human upper and central respiratory system: a validation study, R. Soc. Open Sci. 4 (12) (2017) 170873. doi:10.1098/rsos.170873.

[18] S. Hapuarachchige, Y. Kato, E. J. Ngen, B. Smith, M. Delannoy, D. Artemov, Non-Temperature Induced Effects of Magnetized Iron Oxide Nanoparticles in Alternating Magnetic Field in Cancer Cells, PLoS One 11 (5) (2016) e0156294. doi:10.1371/journal.pone.0156294.

[19] M. Roet, S.-A. Hescham, A. Jahanshahi, B. P. F. Rutten, P. O. Anikeeva, Y. Temel, Progress in neuromodulation of the brain: A role for magnetic nanoparticles?, Prog. Neurobiol. 177 (2019) 1–14. doi:10.1016/j.pneurobio.2019.03.002.

[20] A. Montagne, A. M. Nikolakopoulou, Z. Zhao, A. P. Sagare, G. Si, D. Lazic, S. R. Barnes, M. Daianu, A. Ramanathan, A. Go, E. J. Lawson, Y. Wang, W. J. Mack, P. M. Thompson, J. A. Schneider, J. Varkey, R. Langen, E. Mullins, R. E. Jacobs, B. V. Zlokovic, Pericyte degeneration causes white matter dysfunction in the mouse central nervous system, Nat. Med. 24 (2018) 326–337. doi:10.1038/nm.4482.

[21] K. E. Holter, B. Kehlet, A. Devor, T. J. Sejnowski, A. M. Dale, S. W. Omholt, O. P. Ottersen, E. A. Nagelhus, K.-A. Mardal, K. H. Pettersen, Interstitial solute transport in 3D reconstructed neuropil occurs by diffusion rather than bulk flow, Proc. Natl. Acad. Sci. U.S.A. 114 (37) (2017) 9894–9899. arXiv:28847942, doi:10.1073/pnas.1706942114.

[22] E. Syková, C. Nicholson, Diffusion in Brain Extracellular Space, Physiol. Rev. (Oct. 2008).
URL https://journals.physiology.org/doi/full/10.1152/physrev.00027.2007

[23] R. Zwanzig, Nonlinear generalized Langevin equations, J. Stat. Phys. 9 (3) (1973) 215–220. doi:10.1007/BF01008729.

[24] T. Yuan, L. Gao, W. Zhan, D. Dini, Effect of Particle Size and Surface Charge on Nanoparticles Diffusion in the Brain White Matter, Pharm. Res. 39 (4) (2022) 767–781. doi:10.1007/s11095-022-03222-0.

[25] D. F. Meaney, Relationship between structural modeling and hyperelastic material behavior: application to CNS white matter, Biomech. Model. Mechanobiol. 1 (4) (2003) 279–293. doi:10.1007/s10237-002-0020-1.

[26] S. Singh, A. A. Pelegri, D. I. Shreiber, Characterization of the three-dimensional kinematic behavior of axons in central nervous system white matter, Biomech. Model. Mechanobiol. 14 (6) (2015) 1303–1315. doi:10.1007/s10237-015-0675-z.

[27] R. G. Thorne, C. Nicholson, In vivo diffusion analysis with quantum dots and dextrans predicts the width of brain extracellular space, Proc. Natl. Acad. Sci. U.S.A. 103 (14) (2006) 5567–5572. doi:10.1073/pnas.0509425103.

[28] M. Vidotto, D. Botnariuc, E. De Momi, D. Dini, A computational fluid dynamics approach to determine white matter permeability, Biomech. Model. Mechanobiol. 18 (4) (2019) 1111–1122. doi:10.1007/s10237-019-01131-7.

[29] W. Yao, Z. Shen, G. Ding, Simulation of Interstitial Fluid Flow in Ligaments: Comparison among Stokes, Brinkman and Darcy Models, International Journal of Biological Sciences 9 (10) (2013) 1050. doi:10.7150/ijbs.7242.

[30] L. M. Kassem, N. A. Ibrahim, S. A. Farhana, Nanoparticle Therapy Is a Promising Approach in the Management and Prevention of Many Diseases: Does It Help in Curing Alzheimer Disease?, J. Nanotechnol. 2020 (Aug. 2020). doi:10.1155/2020/8147080.

[31] M. Z. Naik, A. V. Salker, Tailoring the super-paramagnetic nature of MgFe2O4 nanoparticles by In3+ incorporation, Mater. Sci. Eng., B 211 (2016) 37–44. doi:10.1016/j.mseb.2016.05.019.

[32] Fundamental Physical Constants from NIST, [Online; accessed 29. Oct. 2022] (May 2019).
URL https://physics.nist.gov/cuu/Constants

[33] COMSOL Documentation, [Online; accessed 29. Oct. 2022] (Oct. 2022). URL https://doc.comsol.com/6.0/docserver/#!/com.comsol.help.comsol/helpdesk/helpdesk.html

[34] J. Estelrich, E. Escribano, J. Queralt, M. A. Busquets, Iron Oxide Nanoparticles for Magnetically-Guided and Magnetically-Responsive Drug Delivery, Int. J. Mol. Sci. 16 (4) (2015) 8070–8101. doi:10.3390/ijms16048070.

[35] E. M. Cherry, P. G. Maxim, J. K. Eaton, Particle size, magnetic field, and blood velocity effects on particle retention in magnetic drug targeting, Med. Phys. 37 (1) (2010) 175–182. doi:10.1118/1.3271344.

[36] J. F. Schenck, The role of magnetic susceptibility in magnetic resonance imaging: MRI magnetic compatibility of the first and second kinds, Med. Phys. 23 (6) (1996) 815–850. doi:10.1118/1.597854.

[37] B. Ramaswamy, S. D. Kulkarni, P. S. Villar, R. S. Smith, C. Eberly, R. C. Araneda, D. A. Depireux, B. Shapiro, Movement of magnetic nanoparticles in brain tissue: mechanisms and impact on normal neuronal function, Nanomed. Nanotechnol. Biol. Med. 11 (7) (2015) 1821–1829. doi:10.1016/j.nano.2015.06.003.

[38] R. Sheervalilou, M. Shirvaliloo, S. Sargazi, H. Ghaznavi, Recent advances in iron oxide nanoparticles for brain cancer theranostics: from in vitro to clinical applications, Expert Opin. Drug Deliv. 18 (7) (2021) 949–977. doi:10.1080/17425247.2021.1888926.

[39] C. Verry, S. Dufort, J. Villa, M. Gavard, C. Iriart, S. Grand, J. Charles, B. Chovelon, J.-L. Cracowski, J.-L. Quesada, C. Mendoza, L. Sancey, A. Lehmann, F. Jover, J.-Y. Giraud, F. Lux, Y. Crémillieux, S. McMahon, P. J. Pauwels, D. Cagney, R. Berbeco, A. Aizer, E. Deutsch, M. Loeffler, G. Le Duc, O. Tillement, J. Balosso, Theranostic AGuIX nanoparticles as radiosensitizer: A phase I, dose-escalation study in patients with multiple brain metastases (NANO-RAD trial), Radiother. Oncol. 160 (2021) 159–165. doi:10.1016/j.radonc.2021.04.021.

[40] K. M. Luly, J. Choi, Y. Rui, J. J. Green, E. M. Jackson, Safety considerations for nanoparticle gene delivery in pediatric brain tumors, Nanomedicine (Jul. 2020). doi:10.2217/nnm-2020-0110.

[41] E. E. Carpenter, Iron nanoparticles as potential magnetic carriers, J. Magn. Magn. Mater. 225 (1) (2001) 17–20. doi:10.1016/S0304-8853(00)01222-1.

[42] S. Mori, P. C. M. van Zijl, Fiber tracking: principles and strategies – a technical review, NMR Biomed. 15 (7-8) (2002) 468–480. doi:10.1002/nbm.781.